

Pressure-induced phase transitions in weak interlayer coupling CdPS₃

Cite as: Appl. Phys. Lett. **120**, 233104 (2022); <https://doi.org/10.1063/5.0089478>

Submitted: 26 February 2022 • Accepted: 26 May 2022 • Published Online: 08 June 2022

Mengmeng Niu, Haowei Cheng, Xianglin Li, et al.



View Online



Export Citation



CrossMark

ARTICLES YOU MAY BE INTERESTED IN

[Recent progress on 2D magnets: Fundamental mechanism, structural design and modification](#)
Applied Physics Reviews **8**, 031305 (2021); <https://doi.org/10.1063/5.0039979>

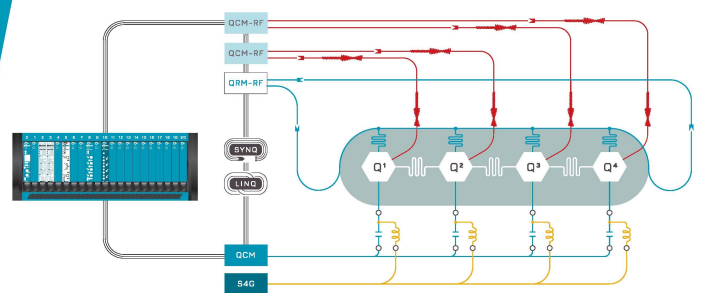
[Anharmonic phonon scattering study in MnPS₃ crystal by Raman spectroscopy](#)
Applied Physics Letters **121**, 032203 (2022); <https://doi.org/10.1063/5.0096814>

[Large out-of-plane piezoelectric response in ferromagnetic monolayer NiClI](#)
Applied Physics Letters **120**, 232403 (2022); <https://doi.org/10.1063/5.0095917>



Integrates all
Instrumentation + Software
for Control and Readout of
Superconducting Qubits

[visit our website >](#)



Pressure-induced phase transitions in weak interlayer coupling CdPS₃

Cite as: Appl. Phys. Lett. **120**, 233104 (2022); doi: 10.1063/5.0089478

Submitted: 26 February 2022 · Accepted: 26 May 2022 ·

Published Online: 8 June 2022



View Online



Export Citation



CrossMark

Mengmeng Niu,¹ Haowei Cheng,¹ Xianglin Li,^{2,3} Jia Yu,¹ Xiaowei Yang,¹ Yuqin Gao,¹ Ruigang Liu,¹ Yang Cao,¹ Kaiyue He,¹ Xiaoji Xie,¹ Qian Shen,¹ Min Lu,¹ Lin Wang,¹  Tingting Yin,⁴ and Jiayu Yan^{1,5,a)} 

AFFILIATIONS

¹Key Laboratory of Flexible Electronics (KLOFE) and Institute of Advanced Materials (IAM), Nanjing Tech University (Nanjing Tech), 30 South Puzhu Road, Nanjing 211800, China

²Hunan First Normal University, No.1015 Fenglin Road (the 3rd), Changsha 410205, China

³Donguan NanoFrontier Microelectronics Equipment Co., Ltd, City of University Innovation, Songshan Lake, Guangdong, China

⁴Division of Physics and Applied Physics, School of Physical and Mathematical Sciences, Nanyang Technological University, 21 Nanyang Link, 637371 Singapore

⁵Changchun Institute of Optics, Fine Mechanics and Physics, Chinese Academy of Sciences, Changchun, Jilin 130000, China

^{a)} Author to whom correspondence should be addressed: yanjiayu@ciomp.ac.cn

ABSTRACT

Metal phosphorus trichalcogenides (MPX₃; M = Fe, Co, Ni, Cd, Mn; X = S or Se) represent a family of two-dimensional (2D) layered materials with an exceptional response to high pressure and a remarkable structural flexibility originating from the weak interlayer coupling. Despite their interest for applications, the knowledge about pressure-driven phase transitions of cadmium compounds is still limited. In this paper, we fill this gap and provide an accurate description of the structural evolution of CdPS₃ by combining high-pressure experiments and first-principle calculations. We have performed high-throughput screening of the low-energy stacking configurations and found a phase evolution starting with *C2/m* space group at 12 GPa using the generalized evolutionary metadynamics method. Then, high-pressure experiments have been used to reveal a structural transition from phase-I (*C2/m*) to phase-II (*R3*) to phase-III (*R3*), which is marked by the appearance and vanishing of the Raman band at approximately 30–250 cm⁻¹ in good agreement with our theoretical predictions. Our study paves the way to the understanding of pressure-induced phase transitions in weak interlayer coupling 2D CdPS₃ materials.

Published under an exclusive license by AIP Publishing. <https://doi.org/10.1063/5.0089478>

Exfoliation of graphene has attracted attention to more general layered materials in condensed matter physics.¹ Beyond graphene, several other compounds have been analyzed, including transitional metal dichalcogenides and black phosphorus, one family of weak van der Waals layered materials, and two-dimensional (2D) transition metal phosphorus trichalcogenides (MPX₃; M = Fe, Co, Ni, Cd, Mn; X = S or Se).^{2–6} MPX₃ members have a structure of atomic S with layers stacked to form a monoclinic *C2/m* phase, whereas Se atomic layers establish trigonal *R3* space groups.⁷ Due to the weaker van der Waals binding between layers, they can form intercalation compounds with various inorganic and organic species and can be used as cathode materials in lithium-ion batteries, as well as photocatalysts for water splitting.^{2–4,8–10} In addition, MPX₃ received attention for their peculiar magnetic properties and anomalous transport behavior.^{11–17}

van der Waals MPX₃ exhibits an exceptional response to high pressure, since the distance between adjacent layers is effectively

reduced, and the electronic properties are modified accordingly.^{18–25} In MnPS₃, three controllable piezochromic behaviors have been found for pressure values above 20 GPa. The symmetry of the structure switches from *C2/m* to *P31m* at approximately 10 GPa and then into another *C2/m* phase above 30 GPa.²¹ MnPS₃ is also characterized by an interesting linear magnetoelectric phase along with an insulator-to-metal transition.²⁴ Recent works have demonstrated that layered FePS₃ undergoes an in-plane lattice collapse and a transition from a monoclinic phase to a trigonal symmetry group, simultaneously accompanied by abrupt spin-crossovers, enhanced electron hopping, and Mott metal-to-insulator transitions under compression.^{18,19,23,25} In addition to the phase transition, superconductivity emerges (below a critical temperature *T_c*) at approximately 2.5 K at 9.0 GPa and the maximum *T_c* at approximately 5.5 K around 30 GPa.^{20,23} All these structural transformations under high pressure are caused by the sliding of layers along different directions.

Despite the above-mentioned findings about the MPX₃ family, only few studies are present about the high-pressure transitions and stability of the corresponding structures for CdPS₃ compounds.²⁶ In this paper, inspired by the remarkable properties of their MPX₃ analog, we analyze in detail the pressure-induced structural transitions of CdPS₃ compounds and present theoretical and experimental results about their dynamics. Our calculations indicate that CdPS₃ had lower cleavage energy compared to other common 2D materials. Guided by the weak interlayer coupling in CdPS₃, the energy of formation of 120 different stacking configurations was compared by artificially sliding along the *x* or *y* direction among stacked layers. In this way, we found the most stable *C2/m* and *R3̄* phases. Then, the structural evolution of CdPS₃ has been studied using a generalized evolutionary metadynamics method at 12 GPa, and the appearance of a *C2/m* to *R3̄* transition, as well as a *P3̄1m* symmetry transformation process has been predicted. *In situ* high-pressure Raman scattering spectra are used to witness the two phase transitions, which are accompanied by the appearance and then vanishing of Raman bands for pressures up to 15.47 GPa in agreement with our theoretical predictions. Overall, our results provide valuable building blocks to study the weak interlayer interaction CdPS₃ crystal and to systematically address MPX₃ structure transition processes under high pressure.

The structural evolution of CdPS₃ under high pressure has been carried out using the generalized evolutionary metadynamics method, as implemented in the evolutionary algorithm Universal Structure Predictor: Evolutionary Xtallography (USPEX) combined with the Vienna *ab initio* simulation package (VASP).^{27–29} Evolutionary metadynamics code is a very powerful method for finding low-energy metastable structures from an established structure.³⁰ We start with an initial structure corresponding to the *C2/m* phase at a given external pressure of 12 GPa. The cell vector matrix h_{ij} was used as a collective variable to monitor the structural changes.³¹ For a given structure with volume *V* and stimulated by an external pressure *P*, the derivative of the free energy with respect to *h* can be expressed as follows:

$$-\frac{\partial G}{\partial h_{ij}} = V[h^{-1}(P - p)]_{ji}. \quad (1)$$

For each generation, equivalent structures are generated and completely relaxed at fixed *h*. The internal pressure tensor *p* is then evaluated for the lowest energy structures. Upon using a stepping parameter δh , the cell shape is updated and the history-dependent Gibbs potential *G*(*t*) is given by

$$G(t) = G^h + \sum W e^{-\frac{|h-h(t')|^2}{2\delta h^2}}, \quad (2)$$

where *W* is the Gaussian height. Then, the vibrational modes for the selected structure are computed and used to produce one more generation of 30 soft-mutated structures. The process is repeated for a number of generations, and a series of structural transitions are observed. The Gaussian width (δh) was set to 0.8 Å and the Gaussian height (*W*) to 3000 kbar Å³.

Ab initio total-energy calculations have been performed on the basis of the density functional theory, as implemented in the PWmat code.³² The DFT-D3 method has been used to analyze the van der Waals interactions³³ with the cutoff energy for plane waves set to 45 Ry. The norm-conserving pseudopotentials and the generalized gradient approximation of the Perdew–Burke–Ernzerhof (PBE)

functional have also been employed.^{34–36} The phonon frequencies at the Γ point and the Raman intensities have been calculated within the density-functional perturbation theory (DFPT)³⁷ as deployed in Phonopy.³⁸ Finally, a $6 \times 4 \times 2$ Monkhorst–Pack *k*-mesh has been used for integration in the irreducible Brillouin zone. To correct the interlayer van der Waals interaction, an optB86b-vdW exchange-correlation functional has been adopted.^{39,40}

CdPS₃ single crystals have been prepared by the chemical vapor transport (CVT) method using high-purity (>99.99%) Cd, P, and S as raw materials. The powder is weighed out with a molar ratio of Cd:P:S = 1:1:3 and homogenized in an agate mortar. The obtained precursor materials are transferred into a quartz ampoule, and then the sealed ampoule is carefully placed into a tube furnace. The source zone and growth zone are kept at 700 and 600 °C, respectively. After the synthesis, x-ray diffraction (XRD) is performed using Cu K α radiation with $\lambda = 1.540598$ Å [Rigaku, SmartLab (3 kW)]. A scanning electron microscope (SEM) (JSM-7800F) equipped with energy-dispersive x-ray spectroscopy (EDS) is used to analyze the samples qualitatively and quantitatively. To generate high pressure, a gasketed membrane-type diamond anvil cell (DAC) is employed with low-fluorescence IA, 500 μ m culet diamonds. The CdPS₃ crystal, together with ruby microspheres, is placed in the center of a 250 μ m sample chamber formed by the gasket and anvil. Silicon oil is introduced as a pressure-transmitting medium, and the ruby microspheres are used to calibrate the pressure exerted on the sample. The Raman spectra are measured using a 488 nm laser excitation (1800 grooves/mm) with the laser beam focused to a spot size of approximately 500 nm (WITec alpha 300R and Princeton Instruments HRS500). To make the sample chamber pressure uniform, after increasing the pressure is maintained for over 60 s.

CdPS₃, like other sulfur derivatives at ambient pressure, crystallizes in a monoclinic phase with four formula units in the crystallographic unit cell and has a layer stacking sequence of inclined AAA. The close-packed sulfur atoms embrace the surfaces within individual layers, and other atoms occupy the center of the octahedron formed by sulfur atoms. Overall, 2/3 of the octahedral positions are filled with Cd²⁺ cations, and the remaining 1/3 are dominated by P2 dimers, as shown in the insets of Fig. 1(a). In order to provide insight into the nature of the weak interlayer coupling of the CdPS₃ crystal, the cleavage energy has been calculated as a function of the separation distance and compared to that of other 2D materials with different structures (graphite, BP, and MoS₂), as shown in Fig. 1(a). The energy gradually increases with the separation distance and then saturates to the cleavage energy of the material. It is worth noticing that the cleavage energy of CdPS₃ (0.17 J/m²) is much smaller than that of BP (0.72 J/m²), MoS₂ (0.55 J/m²), and graphite (0.34 J/m²), clearly indicating the ultraweak interlayer interaction in CdPS₃.

In order to further investigate the ultraweak interlayer cleavage energy, a structure-energy mapping diagram has been obtained by calculating the transition energy of a three-layer AAA stacking cubic phase CdPS₃ supercell, as visualized in Fig. 1(b). There, each color block represents the energy difference of diverse stacking structures generated by the artificial slip along different *x* and *y* directions between the layers. By comparing 120 different stacking models, we found that the energy differences may be remarkable, further indicating the weak interlayer coupling. Interestingly, by shifting the different layers, two structures with the lowest energy [dark blue blocks in

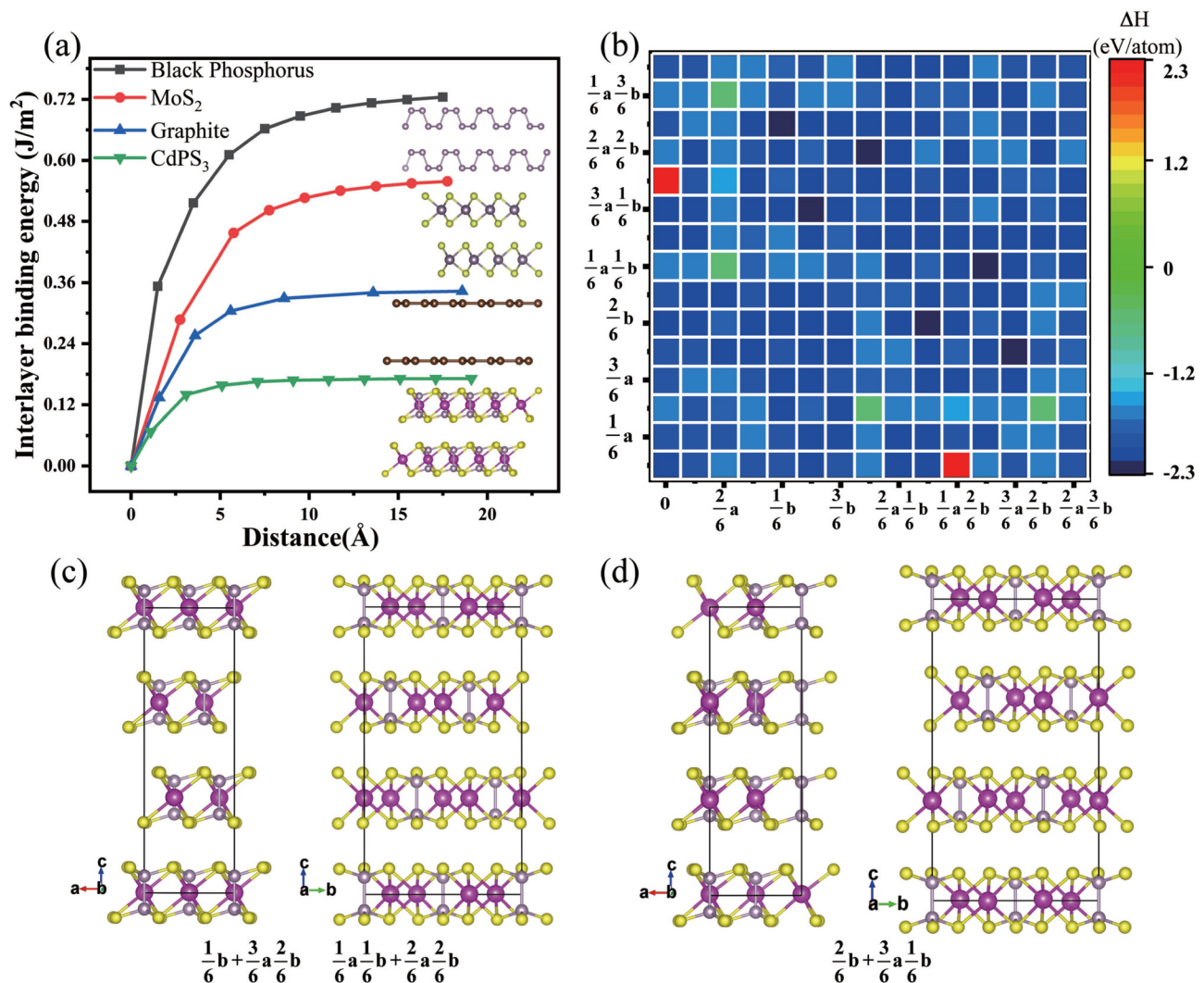


FIG. 1. (a) Calculated interlayer binding energy as a function of the separation distance for typical 2D materials: graphite, BP, MoS₂, and CdPS₃. The insets correspond to their atomic structures. (b) Structure-energy mapping of 120 configurations comprising different stacking sequences. (c) and (d) Lowest-energy structures corresponding to the dark squares in (b).

Fig. 1(b)] have been obtained, and their stacking sequences are exactly the same as those in the $C2/m$ ambient structure and the $R\bar{3}$ low-temperature phase. The operation corresponding to the same stacking of the $C2/m$ phase is $\frac{1}{6}b + \frac{3}{6}a \frac{2}{6}b$ (and $\frac{1}{6}a \frac{1}{6}b + \frac{2}{6}a \frac{2}{6}b$), which means that one layer is shifted by $\frac{1}{6}b$ along the y direction, whereas another layer is shifted by $\frac{3}{6}a$ along the x axis and simultaneously translated by $\frac{2}{6}b$ along the y direction. (One layer is moved by $\frac{1}{6}a$ and $\frac{1}{6}b$ at the same time another layer is shifted by $\frac{2}{6}a$ and $\frac{2}{6}b$.) Similarly, a structure equivalent to the $R\bar{3}$ phase corresponds to $\frac{2}{6}b + \frac{3}{6}a \frac{1}{6}b$ [Figs. 1(c) and 1(d)].

In order to explore phase transitions under high pressure, evolutionary metadynamics calculations have been performed [Fig. 2(a)]. Starting from the $C2/m$ ambient structure, termed phase-I, we found a $R\bar{3}$ structure with lower entropy at generation 46, consistent with

our structure-energy mapping results. This phase is known as the low-temperature phase, and termed phase-II. Interestingly, we found a lightly distorted structure with $R\bar{3}$ space group symmetry at generation 50, and a metastable structure with $P\bar{3}1m$ space group symmetry at generation 8, referred to as phase-III and phase-IV, respectively. Then, taking phase-I as a reference, we have examined the enthalpy differences as a function of pressure up to 25 GPa [as shown in Fig. 2(b)]. Results show that under compression, the structure undergoes a four-stage transition: from phase-I ($C2/m$) to phase-II ($R\bar{3}$), then to phase-III ($R\bar{3}m$), and finally to phase-IV ($P\bar{3}1m$). The first structure transition starts at a pressure as low as approximately 1 GPa, which is consistent with previous results, whereas the phase transition begins at 20 kbar for CoPS₃ and FePS₃ crystals.^{18,41} The second phase transition occurs at 6 GPa while Coak *et al.*¹⁹ found it at approximately 12 GPa

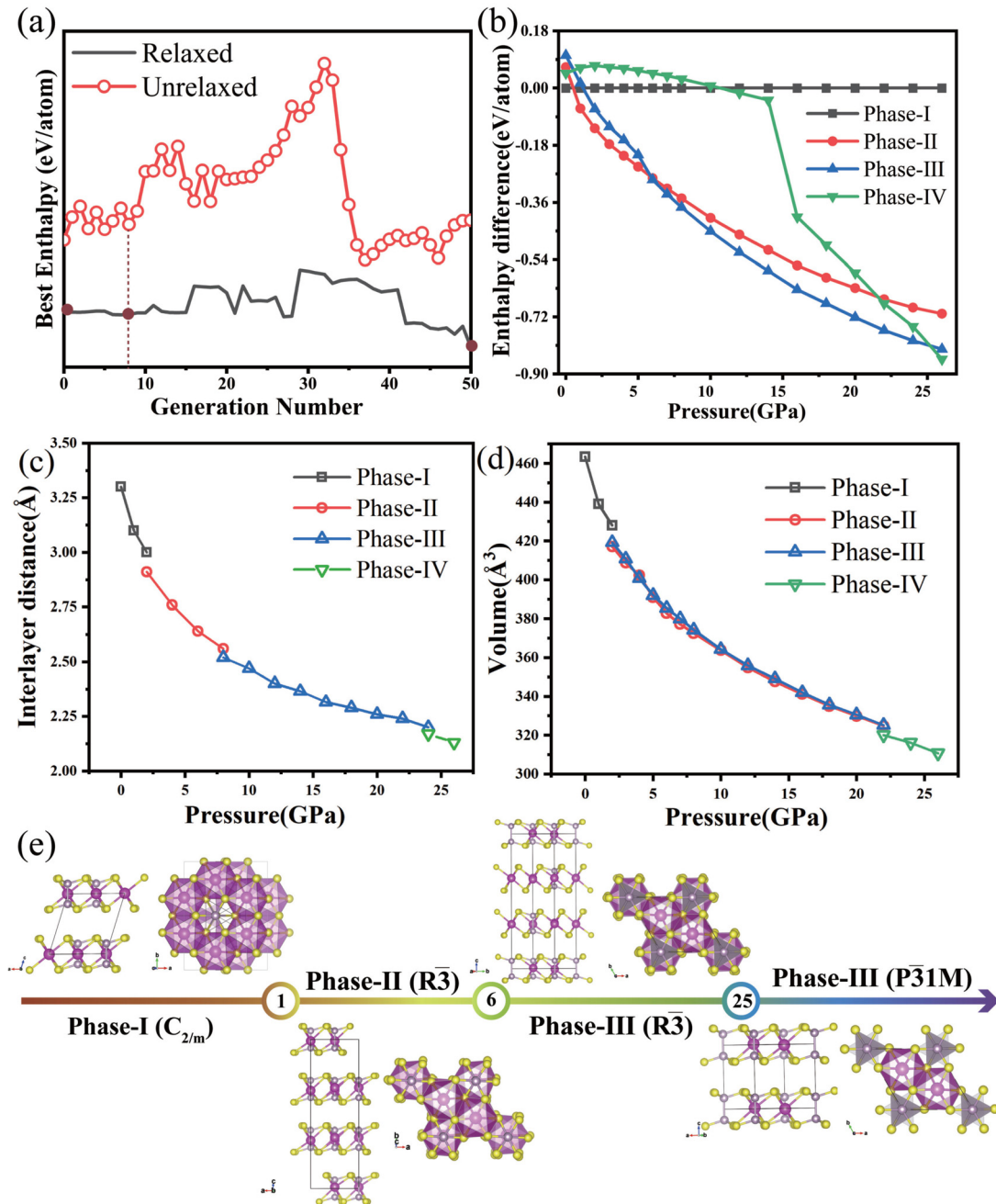


FIG. 2. (a) Enthalpy evolution of CdPS₃ starting with a C_{2/m} space group at 12 GPa using the generalized evolutionary metadynamics method (red line with circles shows enthalpies for possible low-energy structures; black line, enthalpies for best structures after full relaxation). (b) Relative enthalpies of the four predicted phases as a function of pressure (relative to the C_{2/m} structure). The interlayer distances (c) and cell volumes (d) of CdPS₃ vs applied pressures. (e) Phase transition sequence of CdPS₃ at high pressure (magenta spheres, Cd atoms; purple spheres, phosphorus atoms; yellow, sulfur atoms).

for V_{0.9}PS₃ crystals. Similarly, the third transition is observed at approximately 25 GPa, which is close to the MnPS₃ one, occurring at approximately 30 GPa.²¹ We also compared the interlayer distances and cell volumes of CdPS₃ vs applied pressures in Figs. 2(c) and 2(d).

Note that we have normalized the supercell size for more convenient comparison. The interplane lattice parameter shows a steep decrease, indicating the enhanced interlayer interactions. A small cell volume decrease (−2.05% at 2 GPa and −1.46% at 24 GPa) can be seen first,

which is attributed to structural changes from phase-I to the phase-II and phase-III to the phase-IV for CdPS₃. We also calculated the bulk modulus B_0 for each phase. At atmospheric pressure, the bulk modulus B_0 for phase-I (23.95 GPa) is in agreement with the previous obtained data (20.74 GPa in Ref. 42). We did not find any significant volume collapse during the phase transitions. Instead, the members from the MPX₃ family (especially M = Fe, Mn, and Ni) with magnetic states will show a volume collapse of more than 9% during the phase transition under high pressure, which originates from the pressure-driven spin crossover.^{19,23,24} To clarify the dynamics of the transition, we show the atomic structure in Fig. 2(e). A phase-I ($C2/m$) to phase-II ($R\bar{3}$) transition is obtained by sliding a single layer of the atmospheric phase (phase-I) along the y axis for a distance of about $\frac{b}{6}$ and simultaneously sliding it for approximately $\frac{a}{3}$ along the x axis. This results in the $C2/m$ unit's β angle changed from 107.27° to approximately 90° . The phase-II ($R\bar{3}$) to phase-III ($R\bar{3}$) transition is instead caused only by the distortion of CdS₆ polyhedrons. The third transition is due to a relative slip of $\frac{a}{3}$ between the layers along the x axis for the $C2/m$ phase with a stacking configuration of AAA. We have tried to verify our conclusions by comparing high-pressure XRD data from other members of the MPX₃ family. Most of the studies did not reveal the exact structural phase transitions under high pressure due to the low quality of the high-pressure XRD patterns.^{23,24} Haines proposed a HP-I phase with space group $C2/m$ for FePS₃⁴³ and then adopted.¹⁹ In general, this phase possesses the same stacking configuration with our predicted phase-IV with smaller supercell size. Our proposed structural phase transition sequence well rationalizes various high pressure phases observed in the experiment and provides more comprehensive information for the phase diagram of the MPS₃ family.

Next, we investigate experimentally the evolution of the CdPS₃ crystal structure under high pressure using DAC [see Fig. 3(a)], which was instrumental in discovering several phenomena under high pressure in WTe₂,⁴⁴ MAPbBr₃ nanocrystals,⁴⁵ 2D FA₂PbI₄ perovskites,⁴⁶

and WSe₂-MoSe₂ heterobilayers.⁴⁷ The samples used in high-pressure experiments are centimeter-sized yellow flake crystals synthesized by the CVT method. SEM-EDS mapping and XRD measurements are used to characterize the crystals. Energy-dispersive x-ray spectroscopy indicated that samples are composed of Cd, P, and S, and the three elements are distributed homogeneously with an approximate 1:1:3 atomic percentage ratio [see Figs. 3(b) and 3(c)]. Furthermore, XRD data [Fig. 3(d)] reveal a high orientation growth in the (001) direction with characteristic diffraction peaks at 13.24° , 26.99° , 41.1° , 56.01° , and 71.82° . More importantly, no extra peaks can be detected, indicating the high purity and good crystallinity of our samples.

To illustrate the evolution of lattice vibrational properties at various hydrostatic pressures, the typical Raman spectra of the CdPS₃ crystal as a function of pressure are shown in Fig. 4 for frequency in the range 20–650 cm^{-1} . As the pressure increases from 0 to 15.47 GPa, the Raman band blue shifts, which is a common phenomenon in layered materials. However, the low-frequency vibrational mode (approximately 80 cm^{-1}) becomes vanishingly weak and is then undetectable at 1.1 GPa. Surprisingly, a Raman band gradually emerges at around 30 cm^{-1} , as shown in Fig. 4, suggesting that the CdPS₃ crystal undergoes a phase transition at approximately 1.1 GPa. A slight pressure stimulus may cause a structural change in CdPS₃, which is again related to the weak interlayer interaction. Another phase transformation may be observed at 10.2 GPa, where the two Raman peaks gradually merge into a single one. As the pressure continued to rise above 15.47 GPa, the Raman signal became weakened and broadened, and this may be the existence of the pressure gradient due to the non-hydrostatic pressure environment caused by the solidified pressure-transmitting media under high pressure. Our experimental results are, thus, in excellent agreement with our theoretical predictions, confirming the phase transition sequence phase-I to phase-II and finally to phase-III.

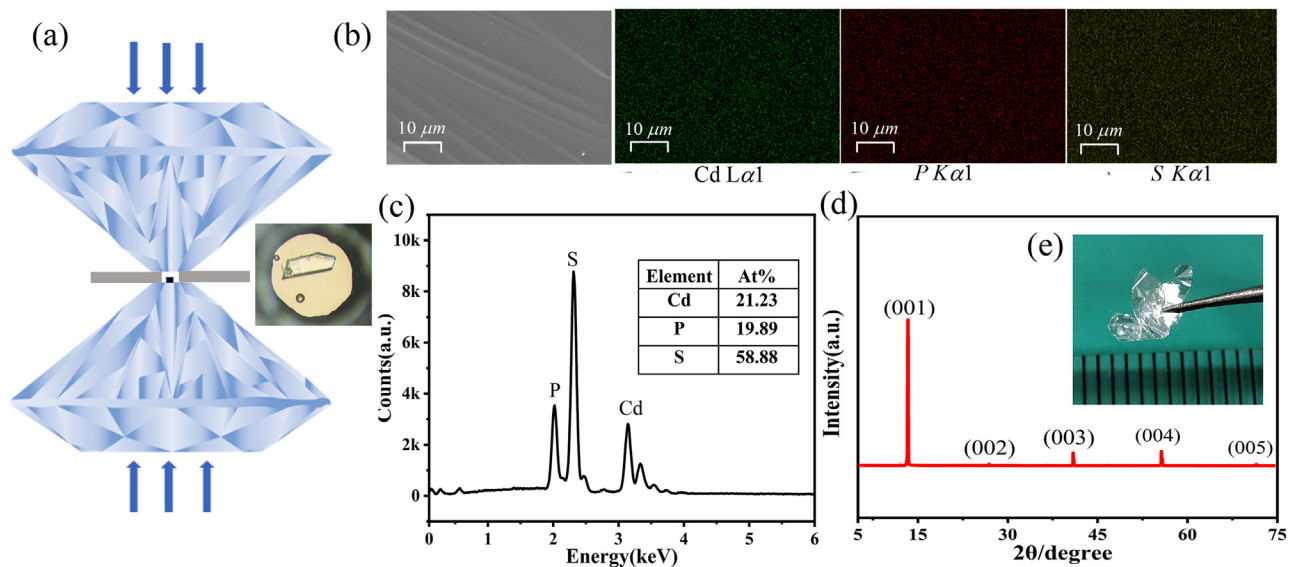


FIG. 3. (a) Schematic of the diamond anvil cell geometry loaded with CdPS₃ crystal and ruby microspheres for the pressure calibration. (b) SEM figure and elemental mapping of Cd, P, and S. (c) EDS image. (d) XRD pattern of synthesized samples. (e) Inset shows the centimeter-sized flake crystals spectrum of our products.

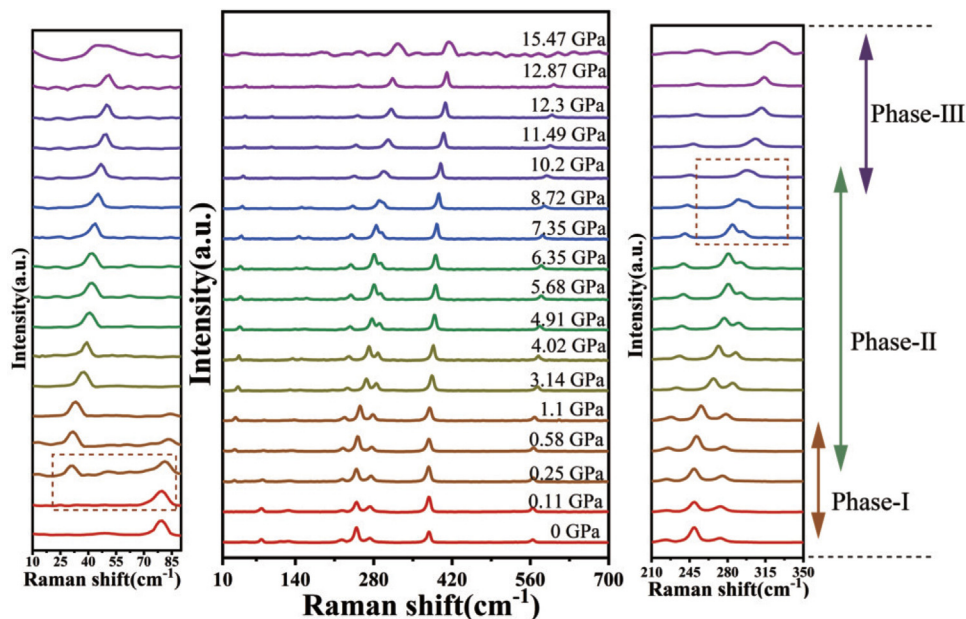


FIG. 4. Evolution of Raman peaks under compression from 0 to 15.47 GPa. Red dashed boxes show the appearance and disappearance of the peaks. The lines mark the phase transition pressures for compressed phase-II and phase-III.

In Fig. 5(a), we show the Raman shift as a function of pressure, which provides intuitive information on anomalous Raman behaviors. The slope of the curve for the three phases differs only slightly, indicating that the Raman band at 249 cm^{-1} is more sensitive to pressure. Modes around 80 cm^{-1} vanishes at 1.1 GPa, which may be attributed to the start of the structural transition. The small slope indicates that the compressibility of the sample decreases with pressure. Although some Raman studies have reported vibration patterns of CdPS₃

crystals, the exact patterns are still unknown, and the Raman shift of approximately 30 cm^{-1} for phase-II is still pending for a full explanation. For this reason, the vibrational modes have been calculated using DFT. The displacements of the Raman-active modes of the CdPS₃ crystal are shown in Figs. 5(b)–5(e). Raman mode vibration associated with the first phase transition is closely related to metal atoms, whereas the second phase transition region is mainly due to sulfur atoms.

In summary, we have profitably combined experiments and theoretical calculations to study the high-pressure phase transitions due to weak interlayer interactions in the CdPS₃ crystal. The structure at high pressure has been interpreted in terms of the slip mechanism between layers. We have employed the generalized evolutionary metadynamics method to seek for possible phases of CdPS₃ at high pressure. The enthalpy spectra have clearly shown a phase-I (*C2/m*) to phase-II (*R $\bar{3}$*) to phase-III (*R $\bar{3}$*) to phase-IV (*P31m*) symmetry transition at 26 GPa. Then, high-pressure experiments have confirmed the structural transitions from phase-I (*C2/m*) to phase-II (*R $\bar{3}$*) to phase-III (*R $\bar{3}$*), which are witnessed by the appearance and vanishing of a Raman band at approximately $30\text{--}250\text{ cm}^{-1}$ in agreement with our theoretical predictions. Our results provide a comprehensive theoretical and experimental description of the phase transitions of MPS₃ materials and pave the way for further developments in the area.

AUTHOR DECLARATIONS

Conflict of Interest

The authors have no conflicts to disclose.

Author Contributions

Mengmeng Niu: Investigation (lead); Writing – original draft (lead). **Haowei Cheng:** Writing – original draft (equal). **Xianglin Li:** Methodology (equal). **Jia Yu:** Investigation (supporting). **Xiaowei Yang:** Methodology (equal). **Yuqin Gao:** Investigation (supporting). **Ruigang Liu:** Investigation (supporting). **Yang Cao:** Investigation

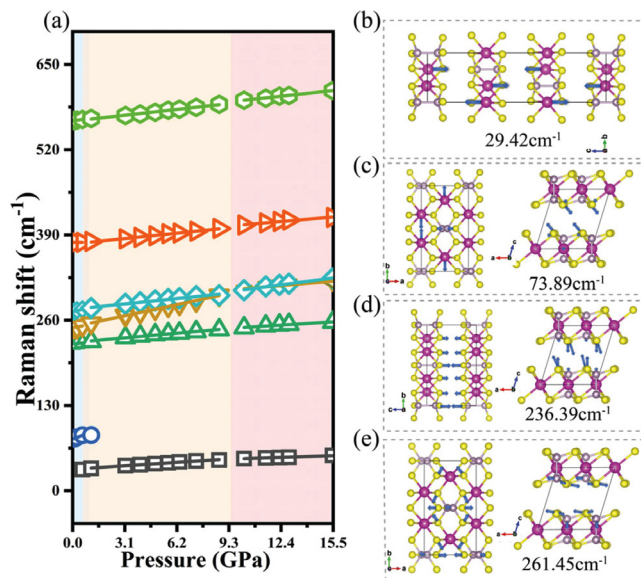


FIG. 5. (a) Raman frequency shifts as a function of pressure. (b)–(e) Typical Raman-active modes of the *C2/m* CdPS₃ crystal.

(supporting). **Kaiyue He:** Investigation (supporting). **Xiaoji Xie:** Supervision (equal). **Qian Shen:** Supervision (equal). **Min Lu:** Supervision (equal). **Lin Wang:** Investigation (supporting). **Tingting Yin:** Methodology (supporting). **Jiaxu Yan:** Conceptualization (lead); Resources (lead); Supervision (lead); Writing – original draft (lead); Writing – review & editing (lead).

DATA AVAILABILITY

The data that support the findings of this study are available from the corresponding author upon reasonable request.

REFERENCES

- ¹K. S. Novoselov, A. K. Geim, S. V. Morozov *et al.*, *Science* **306**, 666 (2004).
- ²M. Barua, M. M. Ayyub, P. Vishnoi *et al.*, *J. Mater. Chem. A* **7**, 22500 (2019).
- ³R. Kumar, R. N. Jenjeti, M. P. Austeria *et al.*, *J. Mater. Chem. C* **7**, 324 (2019).
- ⁴H. Li, N. Wells, B. Chong *et al.*, *Chem. Eng. Sci.* **229**, 116069 (2021).
- ⁵R. Samal, G. Sanyal, B. Chakraborty *et al.*, *J. Mater. Chem. A* **9**, 2560 (2021).
- ⁶F. Wang, T. A. Shifa, P. Yu *et al.*, *Adv. Funct. Mater.* **28**, 1802151 (2018).
- ⁷K. Kurosawa, S. Saito, and Y. Yamaguchi, *J. Phys. Soc. Jpn.* **52**, 3919 (1983).
- ⁸J. Liu, X.-B. Li, D. Wang *et al.*, *J. Chem. Phys.* **140**, 054707 (2014).
- ⁹X. Qian, L. Chen, L. Yin *et al.*, *Science* **370**, 596 (2020).
- ¹⁰X. Zhang, X. Zhao, D. Wu *et al.*, *Adv. Sci.* **3**, 1600062 (2016).
- ¹¹N. Bazazzadeh, M. Hamdi, S. Park *et al.*, *Phys. Rev. B* **104**, L180402 (2021).
- ¹²M. Birowska, P. E. Faria Junior, J. Fabian *et al.*, *Phys. Rev. B* **103**, L121108 (2021).
- ¹³A. Carnabuci, V. Grasso, L. Silipigni *et al.*, *J. Appl. Phys.* **90**, 4526 (2001).
- ¹⁴B. L. Chittari, D. Lee, N. Banerjee *et al.*, *Phys. Rev. B* **101**, 085415 (2020).
- ¹⁵M. Gibertini, M. Koperski, A. F. Morpurgo *et al.*, *Nat. Nanotechnol.* **14**, 408 (2019).
- ¹⁶I. Smaili, S. Laref, J. H. Garcia *et al.*, *Phys. Rev. B* **104**, 104415 (2021).
- ¹⁷D. Vaclavkova, M. Palit, J. Wyzula *et al.*, *Phys. Rev. B* **104**, 134437 (2021).
- ¹⁸M. J. Coak, D. M. Jarvis, H. Hamidov *et al.*, *Phys. Rev. X* **11**, 011024 (2021).
- ¹⁹M. J. Coak, Y.-H. Kim, Y. S. Yi *et al.*, *Phys. Rev. B* **100**, 035120 (2019).
- ²⁰R. A. Evarestov and A. Kuzmin, *J. Comput. Chem.* **41**, 2610 (2020).
- ²¹N. C. Harms, H.-S. Kim, A. J. Clune *et al.*, *npj Quantum Mater.* **5**, 56 (2020).
- ²²H.-S. Kim, K. Haule, and D. Vanderbilt, *Phys. Rev. Lett.* **123**, 236401 (2019).
- ²³Y. Wang, J. Ying, Z. Zhou *et al.*, *Nat. Commun.* **9**, 1914 (2018).
- ²⁴Y. Wang, Z. Zhou, T. Wen *et al.*, *J. Am. Chem. Soc.* **138**, 15751 (2016).
- ²⁵Y. Zheng, X. X. Jiang, X. X. Xue *et al.*, *Phys. Rev. B* **100**, 174102 (2019).
- ²⁶K. Du, X. Wang, Y. Liu *et al.*, *ACS Nano* **10**, 1738 (2016).
- ²⁷A. R. Oganov and C. W. Glass, *J. Chem. Phys.* **124**, 244704 (2006).
- ²⁸C. W. Glass, A. R. Oganov, and N. Hansen, *Comput. Phys. Commun.* **175**, 713 (2006).
- ²⁹G. Kresse and J. Furthmüller, *Phys. Rev. B* **54**, 11169 (1996).
- ³⁰Q. Zhu, A. R. Oganov, and A. O. Lyakhov, *CrystEngComm* **14**, 3596 (2012).
- ³¹M. Parrinello and A. Rahman, *Phys. Rev. Lett.* **45**, 1196 (1980).
- ³²W. Jia, J. Fu, Z. Cao *et al.*, *J. Comput. Phys.* **251**, 102 (2013).
- ³³S. Grimme, J. Antony, S. Ehrlich *et al.*, *J. Chem. Phys.* **132**, 154104 (2010).
- ³⁴J. P. Perdew, K. Burke, and M. Ernzerhof, *Phys. Rev. Lett.* **77**, 3865 (1996).
- ³⁵P. E. Blöchl, *Phys. Rev. B* **50**, 17953 (1994).
- ³⁶G. Kresse and D. Joubert, *Phys. Rev. B* **59**, 1758 (1999).
- ³⁷M. Lazzeri and F. Mauri, *Phys. Rev. Lett.* **90**, 036401 (2003).
- ³⁸A. Togo and I. Tanaka, *Scr. Mater.* **108**, 1–5 (2015).
- ³⁹J. Klimeš, D. R. Bowler, and A. Michaelides, *J. Phys.: Condens. Matter* **22**, 022201 (2010).
- ⁴⁰J. c v. Klimeš, D. R. Bowler, and A. Michaelides, *Phys. Rev. B* **83**, 195131 (2011).
- ⁴¹Y. Gu, S. Zhang, and X. Zou, *Sci. China Mater.* **64**, 673 (2021).
- ⁴²V. Wang, Y.-Y. Liang, Y. Kawazoe *et al.*, *arXiv:1806.04285* (2018).
- ⁴³C. R. S. Haines, M. J. Coak, A. R. Wildes *et al.*, *Phys. Rev. Lett.* **121**, 266801 (2018).
- ⁴⁴J. Xia, D. Li, J.-D. Zhou *et al.*, *Small* **13**, 1701887 (2017).
- ⁴⁵T. Yin, Y. Fang, W. K. Chong *et al.*, *Adv. Mater.* **30**, 1705017 (2018).
- ⁴⁶T. Yin, B. Liu, J. Yan *et al.*, *J. Am. Chem. Soc.* **141**, 1235 (2019).
- ⁴⁷J. Xia, J. Yan, Z. Wang *et al.*, *Nat. Phys.* **17**, 92 (2021).